

Exploring the undrained induced anisotropy of Hostun RF loose sand

T. Doanh · Ph. Dubujet · G. Tournon

Received: 12 April 2010 / Accepted: 18 August 2010 / Published online: 17 September 2010
© Springer-Verlag 2010

Abstract The effects of recent history on the undrained behaviour of very loose and saturated Hostun RF clean sand are investigated in this paper. From an initial isotropic stress state in the triaxial plane, recent histories are generated by isotropic consolidation followed by standard drained triaxial preshear in compression, up to a desired value of axial strain or mobilized stress ratio, and unloading to an initial stress ratio. Subsequent undrained behaviour in triaxial compression is analysed in detail. This paper contributes to the traits explaining the progressive transformation of a compressive and unstable behaviour of loose sand into a dilative and stable behaviour of dense-like sand by previous history, while remaining in the same state of loose density. Experiments show a large pseudo-elastic domain induced by recent history in terms of effective stress paths, function of the initially mobilized stress ratio level, a unique initial gradient of the effective stress paths depending on the stress ratio at the beginning of the undrained shearing, a progressive appearance of dilatancy and a surprising evolution the undrained behaviour of loose sand. Experimental results evidence the important role of the recent deviatoric strain history, from any initial isotropic or anisotropic stress state. This paper also offers a comprehensive understanding of the history mechanisms

created by simple linear stress paths with fixed direction in the classical triaxial plane.

Keywords Anisotropy · Elasticity · Laboratory tests · Liquefaction · Sands

1 Introduction

From the early days of soil mechanics, anisotropy has been recognized as a striking feature of soil behaviour, and it still remains a puzzling subject for both theoretical and experimental scientists, Muir Wood [40]. Inherent and induced anisotropy has been introduced as the two main forms. Inherent anisotropy is often related to the initial fabric of the natural soil skeleton created by the vertical and one-dimensional sedimentation, while induced anisotropy refers to the structural anisotropy resulting from an application of shear deformation.

The effects of anisotropy can be arbitrarily divided into two components $\Psi = \Psi_{\text{induced}} + \Psi_{\text{inherent}}$ and the induced anisotropy separated into two sub-components of stress-induced and strain-induced anisotropy $\Psi_{\text{induced}} = \Psi_{\varepsilon} + \Psi_{\sigma}$. Despite the arbitrariness of this division into multiple and independent mechanisms since the stress and strain are closely related, it can be useful for a better understanding of the involved mechanisms.

In the geotechnical literature, a large number of intensive experimental studies have been devoted to induced anisotropy of granular material. First, conventional triaxial apparatus was largely used by Poorooshasb et al. [32, 33], Tatsuoka and Ishihara [36], Ishihara and Okada [23, 22, 24], Vaid et al. [39] among others, to study the effects of stress-induced anisotropy on the subsequent drained and undrained behaviour of dense sand. One of the objectives

T. Doanh (✉)
Laboratoire Géomatériaux, Ecole Nationale des Travaux Publics
de l'Etat, FRE 3237, 2 Rue M. Audin,
69518 Vaulx en Velin Cedex, France
e-mail: thiep.doanh@entpe.fr

Ph. Dubujet · G. Tournon
Laboratoire de Tribologie et Dynamique des Systèmes,
UMR 5513, Ecole Nationale d'Ingénieurs de Saint-Etienne,
58 Rue J. Parot, 42023 Saint-Etienne Cedex 2, France

was to identify the yield surface within the light of the elastoplasticity framework. Then, in the following decades, with advances in measurements and control techniques, complex machines such as true triaxial, Arthur and Menzies [1], hollow cylinder, Hight et al. [18], and plane strain machines, Tatsuoka et al. [37] for example, were used to explore further the role of induced anisotropy, principal stress rotation, and intermediate principal stress. The main experimental finding was the paramount role of the first stress loading since it considerably alters the mechanical properties of the soil and since induced anisotropy seems to be related to the previous strain history. History strain-dependent mechanisms were introduced in constitutive modelling, and in principle, induced anisotropy can be reasonably described. However, in practice, exactly how and how far to describe the history dependence is still a matter of ongoing debate.

After decades of deciphering the mechanisms of induced anisotropy on dense sand, the potential of using loose density and undrained shearing came into focus. Lanier et al. [28], Doanh and Ibrahim [9], and Gajo and Piffer [14] noticed the same important effect of drained preloading histories on the undrained shear strength of isotropically consolidated samples of Hostun RF sand. For example, after being preloaded drained in compression (resp. extension), sand can liquefy in triaxial extension (resp. compression) regardless of the initial density, whether loose or very dense; contrasting the partial static liquefaction phenomenon usually associated with very loose sand. Similar results were reported for a medium Ottawa sand being preloaded undrained with a more complicated stress history by Vaid [39].

How to quantify the effects of induced anisotropy is the main and still open question, after decades of intensive theoretical and experimental researches. Even when restricted to simple case of linear stress history in the classical triaxial plane, how far is the necessary length of the previous stress history to develop an observable effect, or how to separate the effects of stress history Ψ_σ or strain history Ψ_ϵ with a suitable experimental work? A partial answer to these questions can have significant effects towards a better understanding of the mechanisms underlying the induced anisotropy. The previous works, [8], show the progressive transformation of a compressive and unstable behaviour of loose sand into a dilative and stable behaviour of dense-like sand by previous deviatoric strain history, while being loose within a narrow range of relative density. The change in void ratio alone cannot be a sufficient parameter in explaining this progressive transformation of the observed behaviour.

The purpose of this paper is to present new experimental findings trying to explain this progressive transformation. An extensive programme on very loose and saturated

Hostun RF sand was especially designed to explore the effects of previous stress and strain history. Recent histories are created by simple linear stress paths with fixed direction from an initial isotropic stress state in the classical triaxial plane and performed on sand samples having nearly the same initial void ratio prior to undrained shearing. In this paper, partial drained unloading in compression from different mobilized stress ratios is considered.

2 Experimental programme

The undrained behaviour of loosely and normally consolidated sand was first investigated by Canou et al. [4], Meghachou [31], Konrad [25], Ibrahim [20]. Lightly, overconsolidated behaviour was logically studied next by Di Prisco et al. [6], Matiotti [30], Gajo and Piffer [14], followed by recent works on K -consolidated state by Finge et al. [11] examining some effects of the induced anisotropy generated by constant effective stress ratio paths. The characteristics of loose sand, in its loosest density provided by moist tamping technique, change dramatically with the direction of previous loading and shearing mode, even when restricted to the classical triaxial plane.

The essential features of the undrained induced anisotropy of loose sand of a previous work, [7], are presented in Fig. 1. Dashed lines represent the effective stress paths of three representative samples being drained sheared in compression up to a deviatoric level q_{mob} and immediately undrained sheared also in compression. Loose sand samples are unable to sustain the imposed deviatoric stress q_{mob} , resulting in a contractive flow behaviour with increasing pore pressure of unstable response often termed “static liquefaction”. Full lines show the undrained behaviour of sand samples following a full drained cycle, i.e. drained loading to q_{mob} and drained unloading to the same initial isotropic stress state. They indicate different responses of subsequent monotonic undrained loading with a dilative and eventually stable behaviour with decreasing pore pressure. It is worth noting that all samples have nearly the same relative density at the beginning of undrained loading to minimize the effects of density. The response of a virgin isotropic loose sample is also superimposed as dotted line for comparison, offering the usual static liquefaction behaviour.

This experimental work indicates that the compressive and unstable behaviour of loose sand (dashed lines) can be progressively transformed into a dilative and stable behaviour of dense-like sand (full lines) by previous deviatoric strain history while being loose within a narrow range of relative density.

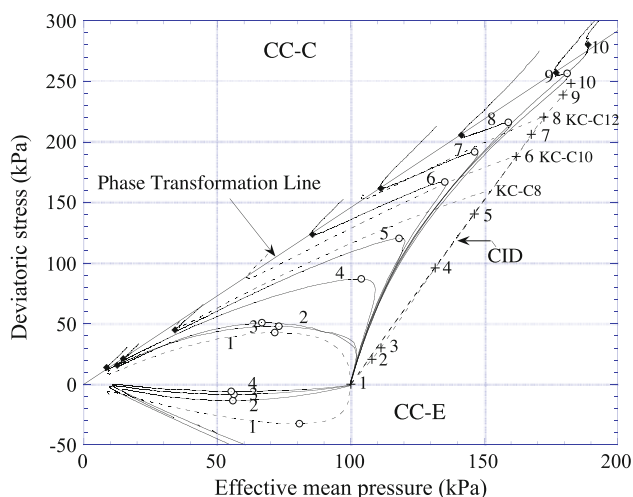


Fig. 1 Undrained induced anisotropy of loose sand

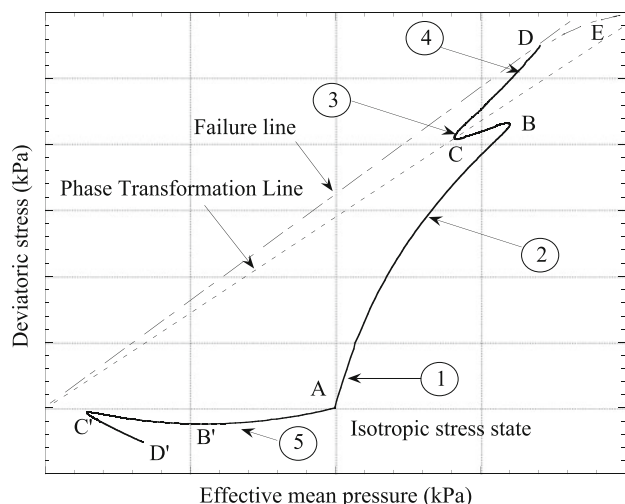


Fig. 2 Schematic illustration of the effects of undrained induced anisotropy of loose sand

Figure 2 summarizes the salient features of the current knowledge of the observed behaviours showing schematically with 5 open circles : **(O1)** the directional dependency of the initial effective stress gradient, **(O2)** the pseudo-elastic response, **(O3)** the progressive appearance of the dilatancy domain, **(O4)** the evolution of the undrained behaviour, and **(O5)** the systematic static liquefaction associated with small undrained strength when sheared in the opposite direction of the initial presheared direction. The last observation is left aside in this paper since all samples are drained presheared in compression and subsequently undrained sheared in the same direction.

Once identified the effect of previous deviatoric strain history, the next logical step is to characterize the effect of

recent stress history on the same sand with the same relative density. This paper proposes to explore the mechanisms of undrained induced anisotropy on Hostun RF loose sand with new sets of partially drained unloading levels from four fixed mobilized stress ratio η_{mob} and uses the identified mechanisms, developed for Hostun loose sand in Doanh et al. [7], as background for evaluating new experimental results. The unloading stress ratios η_c are carefully chosen to contribute to the traits that bridge the gap between the observed behaviours in Fig. 1.

The sand employed in this study is the Hostun RF fine-grained silica clean sand. It is a reference sand for many French geotechnical laboratories and it also is widely studied in the international geotechnical community. It consists of subangular grains having a specific gravity equal to 2.65. This sand has the minimum e_{min} and the maximum e_{max} void ratios of 0.624 and 0.961 and a uniformity coefficient of 1.9. Many other properties can be found at Flavigny et al. [12].

The experimental works were conducted using a modified classical triaxial system. All tests were axially loaded in a strain-controlled mode with a deformation rate of about 0.21%/min. The axial load and displacement were measured inside the triaxial cell by a submersible load cell and by a linear variable differential transformer (LVDT) sensor mounted directly on the top platen. The pore-water pressure was measured near the top cap of the sand sample since the back pressure was applied at the bottom.

The modifications, the sample preparation, and the saturation are given in previous works [9, 20, 10]. The initial void ratio determination, the repeatability of the undrained test, and the verification of the antifrictional system were checked in [8, 17].

A modified moist tamping and under compaction method, inspired by the early works of Bjerrum et al. [3] and Ladd [26], was employed to prepare very loose and contractive sand samples at fabrication stage. Although the moist-tamped sand cannot simulate the natural deposited sand, Frost and Park [13], it can constitute a useful laboratory step towards a better understanding of the latter.

Short samples, 70 mm in height and 70 mm in diameter, enclosed within a latex membrane of 0.3 mm of thickness were prepared with enlarged and lubricated end plates to produce homogeneous deformations at large strains. A total of 5 layers of predetermined equal weight of moist sand were compacted into prescribed thickness using a tamping circular stainless steel rod. To minimize the effect of density on the observed undrained behaviour, special attention was given to have samples with nearly identical void ratios at the beginning of undrained shearing. The initial void ratio of all samples at fabrication state, e_0 , was around 1.03, in order to have a relative density D_r of very loose sand, less than 15%, before undrained shearing.

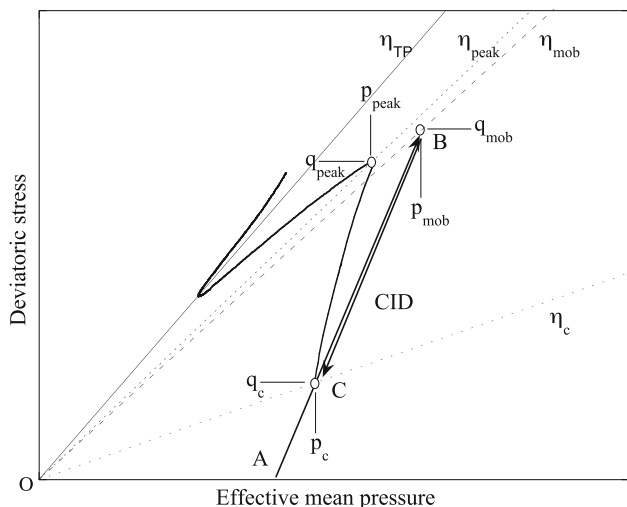


Fig. 3 Different preloading stress paths

2.1 Preloading histories

Different preloading histories in Fig. 3 were chosen to clarify the effects of the undrained induced anisotropy of fully saturated sand samples. Loose sand samples were isotropically consolidated to point A, then drained loaded in triaxial compression up to point B having mobilized stress ratio level η_{mob} , and drained unloaded down to point C with a stress ratio level η_c before the final undrained shearing in compression. The investigated points C_i are distributed along the whole unloaded part AB in order to bridge the gap between the surprising observed behaviour at point A, with complete unloading to the initial isotropic stress state, and the behaviour at point B, without drained unloading. The direction of all preloading histories is fixed, $\alpha = 71^\circ$, from the positive mean effective pressure axis.

Following previous study [7], four mobilized stress ratios level η_{mob} are selected: lightly below ($\eta = 0.60$) and above (0.75) the instability line (0.64) of virgin isotropically and normally consolidated sand, close (1.15) and very close (1.40 or 90%) to the undrained failure (1.50), defined later in 3.1. The values of axial strain attained during the drained compression loading and partially unloading can be large, up to +12% in compression.

For each mobilized stress ratios level η_{mob} above, four levels of drained unloading η_c are also of interest : complete unloading (0.0), below and above the instability line (0.35 and 0.75), and near the undrained failure (1.13).

2.2 Void ratio before undrained shearing

The initial isotropic hypothesis ($\epsilon_{vol} = 3.0 \epsilon_{axial}$) of sand samples over the studied stress range was checked in a previous study [11] with a gradient $\epsilon_{vol}/\epsilon_a$ is 2.97 ± 0.30

Table 1 Relative density of different series

Series, η_{mob}	D_r (%)
0.60	8.90 ± 2.97
0.75	5.86 ± 3.73
1.15	12.66 ± 0.58
1.40	16.15 ± 3.09

in isotropic loading and 3.32 ± 0.36 during isotropic unloading. Table 1 shows the average relative density at the end of the preloading history. The target of loose sand before undrained shearing is satisfied, i.e less than 15% of D_r , excepting some tests with largest mobilized stress ratios level $\eta_{mob} = 1.40$. The variability of the void ratio e_c at the end of the preloading history before undrained shearing seems to be randomly distributed within each series of fixed η_{mob} .

Table 2 summarizes all tests of this study with their initial conditions and their results. The first letter “C” in the test name indicates the drained standard triaxial compression preshear; the second “C” is the final undrained shearing mode in compression. e_{0-20} is the void ratio at 20 kPa of effective confining pressure after the completion of saturation, e_{0-100} at the end of the isotropic consolidation stage at 100 kPa and $\epsilon_{dev}^c = \epsilon_a^c - \epsilon_r^c$ the deviatoric strain at the beginning of undrained shearing at η_c , where ϵ_a and ϵ_r (σ'_a and σ'_r) are the axial and radial strain (effective stresses). The zero strain state is chosen at the beginning of undrained loading.

3 Undrained behaviour of presheared loose sand

The test results were interpreted in terms of the deviatoric stress $q = \sigma'_a - \sigma'_r$ and the effective mean pressure $3p' = \sigma'_a + 2\sigma'_r$. The effective stress ratio is defined as $\eta = q/p'$. The stress paths were examined in the $q - p'$ plane and the response behaviour mainly in the deviatoric–axial strain plane and in the normalized excess pore pressure ΔU was normalized by the initial effective radial stress before the final monotonic undrained shearing. A virgin isotropic sample is superimposed as dashed line in all figures to facilitate the visual comparison. Anisotropic scale is used to emphasize the differences in the response of virgin, partial, and complete drained unloading behaviours. The results of the drained preloading can be found at Touron [38].

For each series in Table 2, the mobilized stress ratios level η_{mob} is fixed with variable levels of drained unloading η_c or variable initial stress states before undrained loading.

Table 2 Undrained tests on loose and partially presheared Hostun sand

Tests	$e_{0.20}$	$e_{0.100}$	e_c	D_{r_c}	η_{mob}	η_c	$\eta_{peak}\%$	ε_{peak}	η_{TP}	$\varepsilon_{dev}^c\%$
$\eta_{mob} = 0.60$ (40% of undrained failure)										
C 0.60–C1	0.948	0.929	0.921	11.87	0.75	0.00	0.73	0.15	1.26	0.62
C 0.60–C2	0.961	0.940	0.931	8.90	0.75	0.37	0.68	0.07	1.51	0.76
C 0.60–C3	0.971	0.948	0.941	5.93	0.75	0.58	0.67	0.04	1.68	0.61
$\eta_{mob} = 0.75$ (50% of undrained failure)										
C 0.75–C1	0.966	0.940	0.926	10.39	0.75	0.00	0.85	0.15	1.40	0.86
C 0.75–C2	0.984	0.971	0.956	1.48	0.75	0.35	0.81	0.08	1.37	1.31
C 0.75–C3	0.973	0.951	0.938	6.82	0.75	0.41	0.82	0.07	1.36	1.20
C 0.75–C4	0.983	0.960	0.945	4.75	0.75	0.73	0.79	0.02	1.42	1.23
$\eta_{mob} = 1.15$ (77% of undrained failure)										
C 1.15–C1	0.982	0.961	0.922	11.57	1.16	0.01	1.24	0.56	1.43	5.47
C 1.15–C2	0.973	0.952	0.917	13.06	1.15	0.36	1.21	0.19	1.45	4.40
C 1.15–C3	0.979	0.957	0.919	12.46	1.15	0.45	1.20	0.19	1.45	5.62
C 1.15–C4	0.972	0.950	0.916	13.06	1.15	0.75	1.20	0.09	1.47	5.19
C 1.15–C5	0.981	0.956	0.917	13.06	1.15	0.97	1.18	0.04	1.46	5.58
C 1.15–C6	0.978	0.952	0.918	12.76	1.15	1.14	1.17	0.01	1.44	5.68
$\eta_{mob} = 1.40$ (90% of undrained failure)										
C 1.40–C1	0.984	0.958	0.895	19.58	1.37	0.01	–	–	–	14.77
C 1.40–C2	0.987	0.964	0.913	14.24	1.38	0.34	–	–	–	15.29
C 1.40–C3	0.973	0.951	0.898	18.69	1.38	0.44	1.43	1.08	1.45	15.05
C 1.40–C4	0.992	0.968	0.905	16.62	1.37	0.73	1.40	0.38	1.46	16.31
C 1.40–C5	1.002	0.979	0.926	10.39	1.38	1.13	1.40	0.07	1.48	12.01
C 1.40–C6	0.980	0.957	0.902	17.51	1.37	1.31	1.38	0.00	1.45	15.67

Consequently, these series emphasize the role of recent stress history, characterized by the length of the loading path or by $\eta_{mob} - \eta_c$.

3.1 Compression preshearing with mobilized level

$\eta_{mob} = 0.75$ near instability line

These first two series featuring a limited number of tests confirmed the well-known undrained instability behaviour of Hostun RF loose sand. In the $q - p'$ plane, the Lade's instability line IL [27], defined for virgin isotropically and normally consolidated sand (marked as dashed line), has a slope in compression $\eta_{LI} = 0.64$ (broken line) or a mobilized frictional angle at peak ϕ_{peak} of about $18^\circ 6'$ in Fig. 4a.

As expected from the instability concept, since the presheared level η_{mob} is below or near the instability line, the effective stress paths reach a small peak (vertical arrow) at small strain followed by a sharp drop of deviatoric stress to a residual value corresponding to the steady state of deformation (SSD [21]) in Fig. 4b. The deviatoric stress increases slightly at large strain, after 8% of axial strain or after a large range of axial strain with constant residual stress of the SSD. A rather temporarily unstable behaviour is observed for all tests of these series.

All effective stress paths follow a very similar pattern evolution, showing an initial nearly parallel and inclined towards the positive p' axis, a linear development within the pseudo-elastic domain (defined later in Sect. 4.2) from the beginning of the undrained shearing, a progressive transition from the pseudo-elastic state to a plastic one around the rounded peak towards a common point H in Fig. 5b at deviatoric stress level of about 90 kPa, a common descending part from point H to the point of phase transformation, and the final climb-up along the undrained failure. Since the deviatoric stress was systematically increased at large strain for all tests, eventually reaching a much larger value at ultimate stress state beyond the capacities of the current equipment, the deviatoric stress at failure was taken at 20% of axial strain to avoid the inhomogeneous strain state at large deformation. All stress states at failure were aligned in the $q - p'$ plane.

The stress path of test C 0.75–C4, without drained unloading, represents an envelope for all drained preshear with η_c smaller than η_{mob} . This limiting stress boundary confirms the previous observations of Gajo and Piffer [14], Doanh et al. [7] on the same loose Hostun RF sand with small mobilized preloading level η_{mob} and Georgiannou et al. [15] on anisotropically consolidated clayey sands.

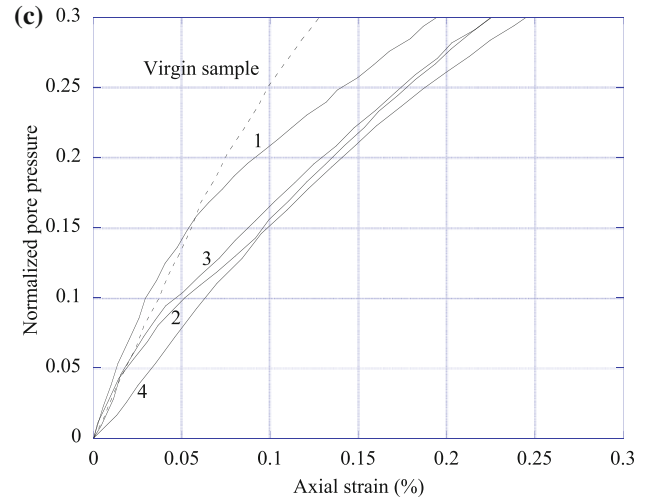
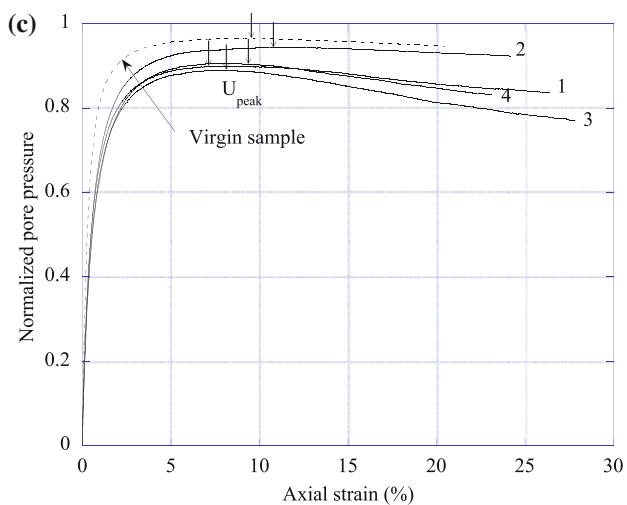
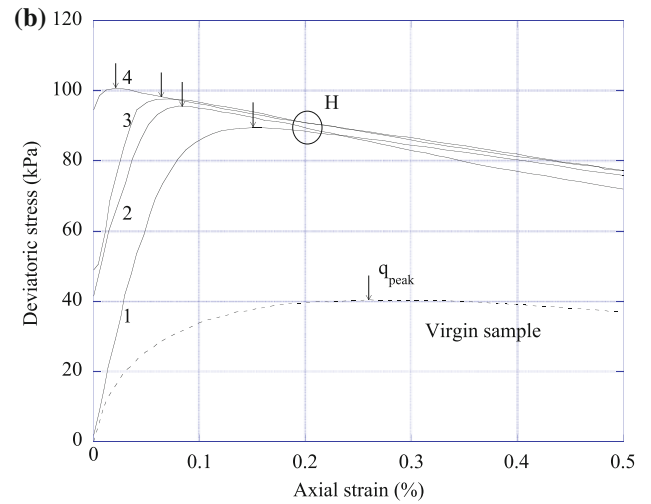
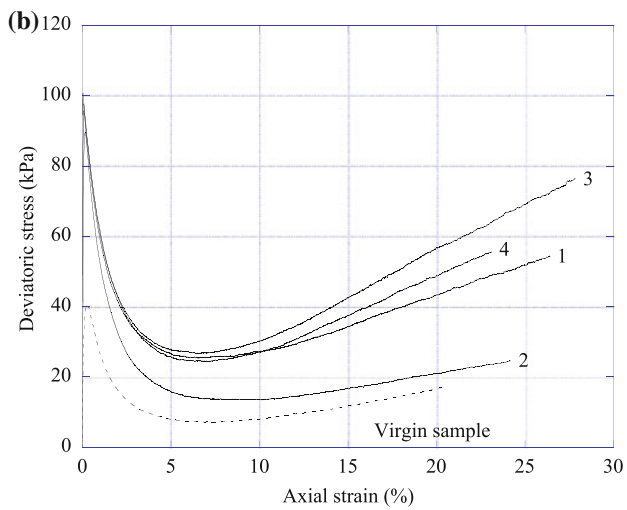
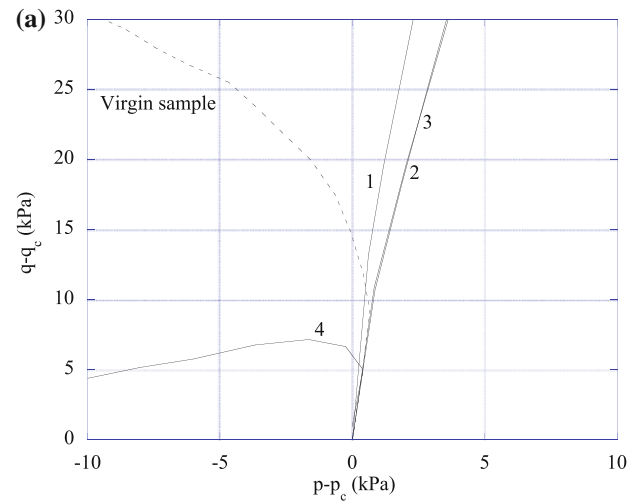
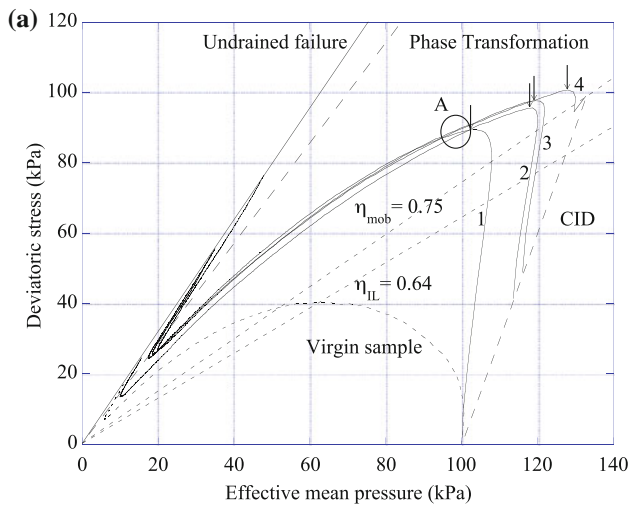


Fig. 4 Results on compression presheared cycle $\eta_{mob} = 0.75$ samples. **a** Effective stress paths. **b** Stress–strain relationships. **c** Pore pressure generation

Fig. 5 Detailed results on compression presheared cycle $\eta_{mob} = 0.75$ samples. **a** Effective stress paths. **b** Stress–strain relationships. **c** Pore pressure generation

The Hill's instability criterion of second-work order [19] is defined as $d^2W = d\sigma_{ij} \cdot d\varepsilon_{ij}$ with $d\sigma_{ij}$ and $d\varepsilon_{ij}$ the incremental stress and strain tensor. In the case of undrained triaxial, it is reduced to $d^2W = d\sigma_a \cdot d\varepsilon_a + 2d\sigma_r \cdot d\varepsilon_r = dq \cdot d\varepsilon_a$. Therefore, d^2W and dq have the same sign for undrained compression. Consequently, loose sand is unstable since d^2W has negative values from deviatoric stress peak q_{peak} to the SSD, and positives values afterwards. Test C 0.75–C4 with $\eta_c = \eta_{mob}$, without drained unloading, has its smallest undrained compressive strength increment, defined as $\Delta q_u = q_{peak} - q_c$, of about 7.1 kPa in Fig. 5a and its largest undrained compressive strength at q_{peak} of 100.3 kPa in Fig. 5b. On the contrary, test C 0.75–C1 with $\eta_c = 0$, with complete drained unloading, has the largest Δq_u and the smallest q_{peak} of 89.4 kPa, and test C 0.75–C2 with partial preshearing offers an intermediate value Δq_u of 53.0 kPa and q_{peak} of 95.5 kPa. The axial strain at peak increases with the size of the unloading stage, passing from 0.021% for sample without unloading to 0.151% for a complete unloading.

Note that localized shear bands have never been observed visually, and the shape of sand sample remains almost cylindrical; the unstable behaviour is associated with a diffuse failure by Darve et al. [5], well below the usual undrained failure.

Typical normalized excess pore pressure at different levels of η_c are shown in Fig. 4c. Without exception, the normalized excess pore pressure developed progressively and continuously with the axial strain and reached a peak in the range of 89 to 93% at large strain followed by a small reduction. The static liquefaction, defined as the ability to reach the origin of the $q - p'$ plane under monotonic shearing conditions, was nearly attainable with virgin sample. However, the behaviour of limited flow with a maximum of excess pore pressure ΔU_{max} was systematically observed for all presheared tests. A less developed pore pressure is noticed for presheared samples, compared to that of virgin sample in Fig. 5c.

All stress–strain relationships of presheared samples are grouped together beyond the axial strain level of about 0.2% in the detail results of Fig. 5b, well above the stress–strain of virgin sample. This observation, together with the common stress path from point A in Fig. 4a, indicates the elimination of the previous linear stress history beyond 0.2% of axial strain. Different developments of stress–strain behaviour at large strains in Fig. 4b are probably due to different internal structures of loose sand.

In the detailed results of Fig. 5a showing the initial gradient of the effective stress path from the beginning of the undrained shearing, a positive gradient is always obtained. This observation suggests a greater stiffness in the vertical direction due logically to the drained

compressive preshearing and conjointly to the existence of an initial deviatoric stress.

Only one partial drained unloading is performed in the series with mobilized presheared level $\eta_{mob} = 0.60$ below the instability line. Since the observed behaviour seems to conform to the expected one, no additional experiment is needed.

3.2 Compression preshearing with $\eta_{mob} = 1.15$

The third series of 6 tests including 4 partial unloadings with higher mobilized level, well above η_{LI} , gives the first opportunity to explore the non-linear behaviour within the pseudo-elastic domain.

Regarding the observed results of the two previous series, the four essential features (O1) to (O4) are still valid with different variations in Fig. 6: an initial nearly parallel and inclined effective gradient with different values, a non-linear development within the pseudo-elastic domain, a transition from the pseudo-elastic state to a plastic one around a progressively sharp deviatoric peak towards a common point, and a limiting stress envelope obtained from sample without unloading. Nevertheless, additional details emerge since this series imposes a relatively high mobilized level η_{mob} , up to 77% of undrained failure, comparing to that of previous series. It is worth noting a different temporarily unstable behaviour, in which the attained maximum of excess pore pressure ΔU_{max} ranges only from 55 to 65% of the initial confining pressure, followed by a larger pore pressure decreasing afterwards.

In Fig. 7a, a sharp peak is noticed, showing a first observed abrupt transition from pseudo-elastic to plastic state. This rare observation offers a support for the decomposition of elastic and plastic parts within the current mainstream of elastoplastic theory. A regular pattern of initial effective stress gradients is also noticed, depending on the value of unloading level η_c . In Fig. 7b, the effects of previous linear stress history became insignificant beyond 0.5% of axial strain; however, its range is well beyond the pseudo-elastic domain delimited by the deviatoric peak. The detail results of Fig. 7c show a new development of ΔU at small strain beside a regular pattern: a first appearance of the local peak of excess pore pressure of test C 1.15–C1 with complete drained unloading.

3.3 Compression preshearing with large mobilized level $\eta_{mob} = 1.40$

The last series of also 6 tests including 4 partial unloadings with highest mobilized level performed in this study, up to 90% of undrained failure, detects a new development, never seen before for smaller mobilized levels.

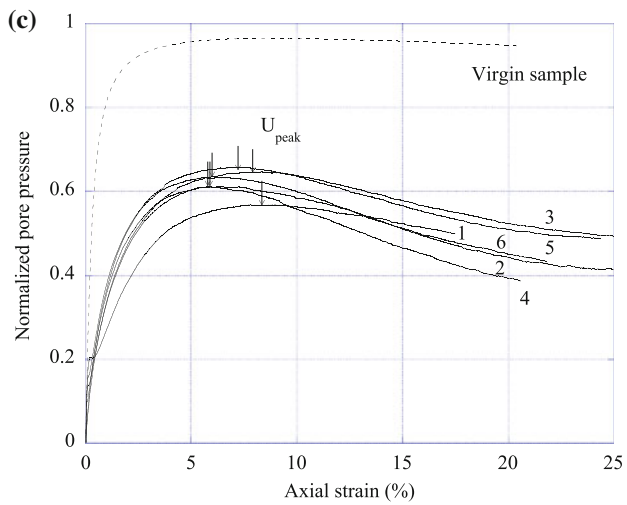
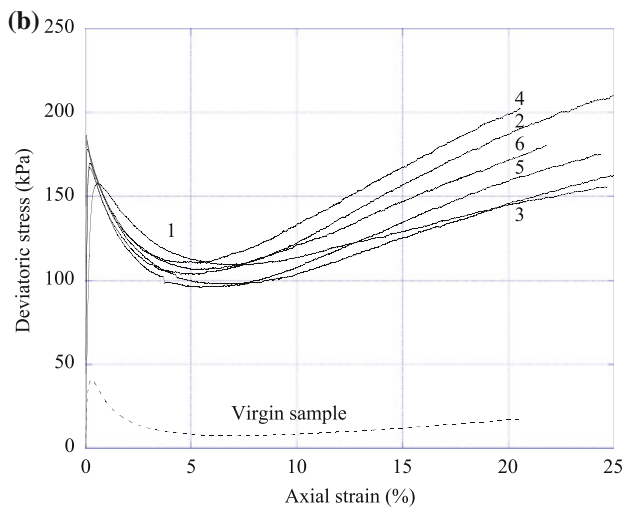
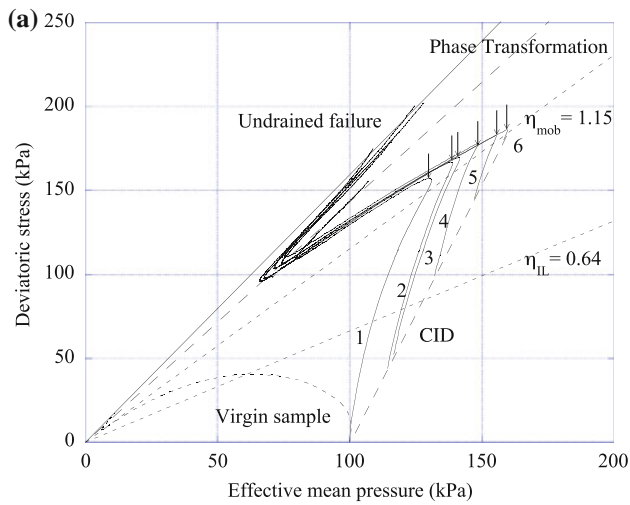


Fig. 6 Results on compression presheared cycle $\eta_{mob} = 1.15$ samples. **a** Effective stress paths. **b** Stress–strain relationships. **c** Pore pressure generation

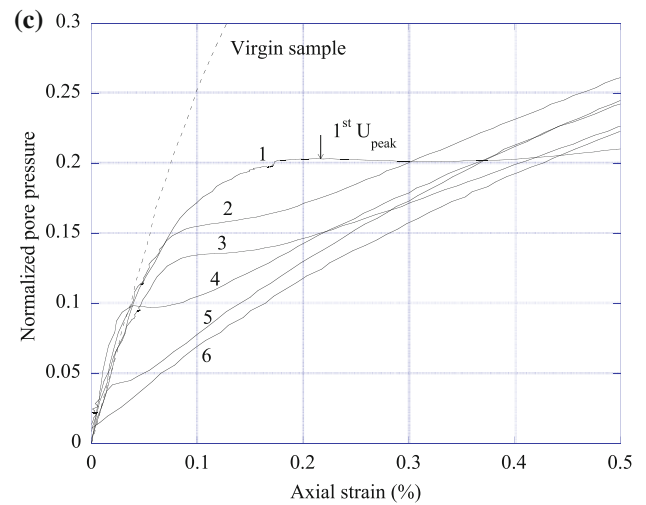
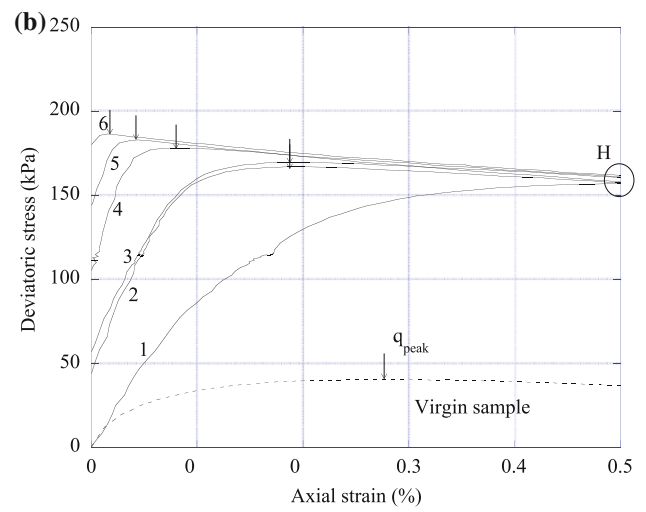
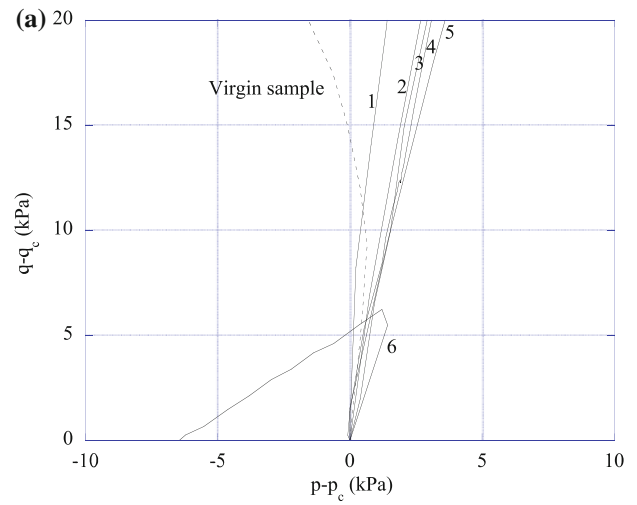


Fig. 7 Detailed results on compression presheared cycle $\eta_{mob} = 1.15$ samples. **a** Effective stress paths. **b** Stress–strain relationships. **c** Pore pressure generation

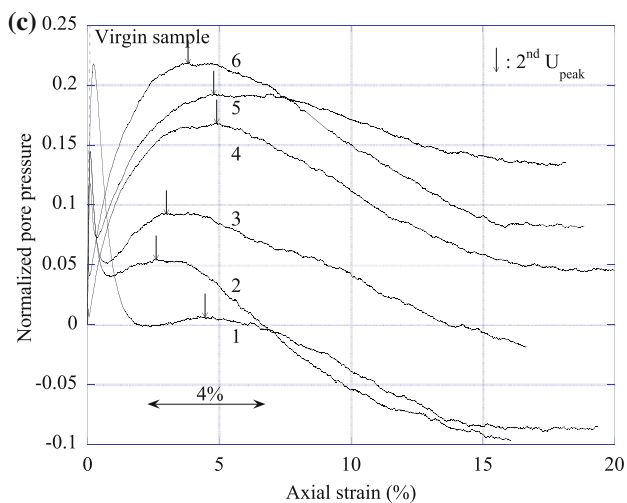
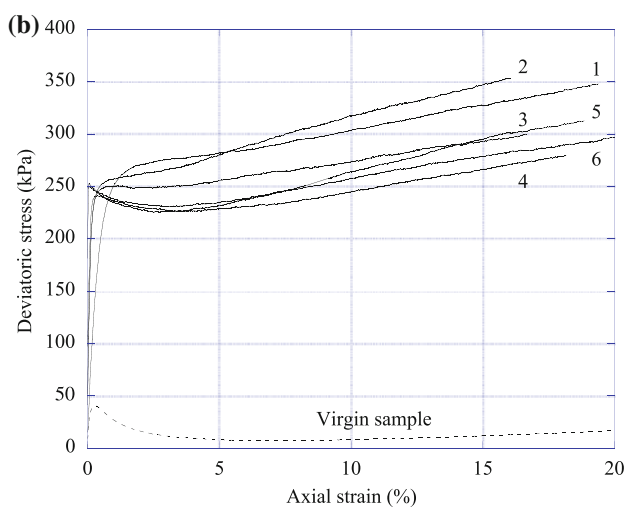
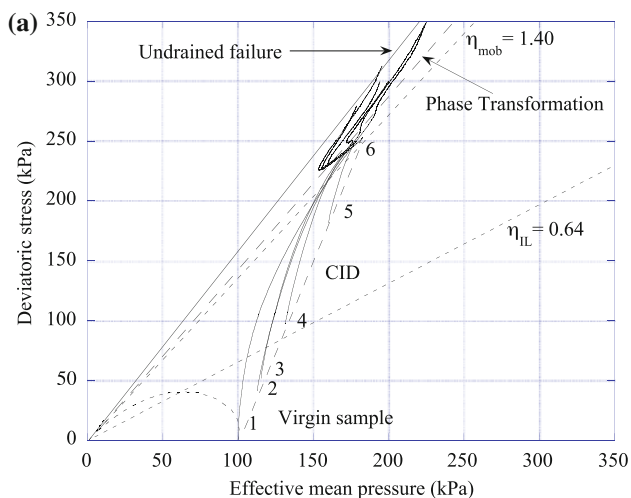


Fig. 8 Results on compression presheared cycle $\eta_{mob} = 1.40$ samples. **a** Effective stress paths. **b** Stress–strain relationships. **c** Pore pressure generation

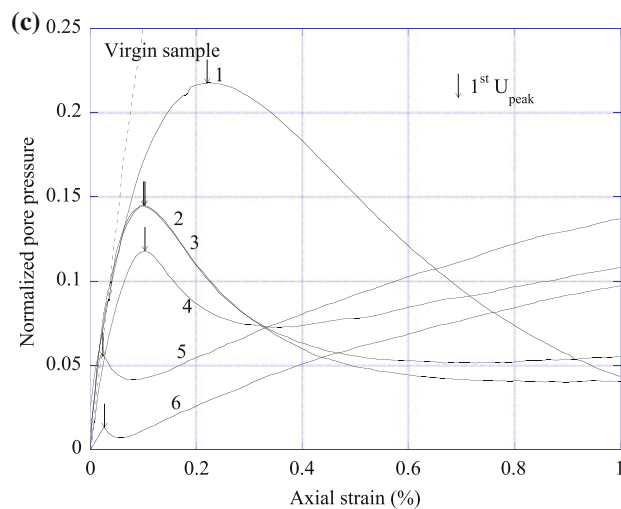
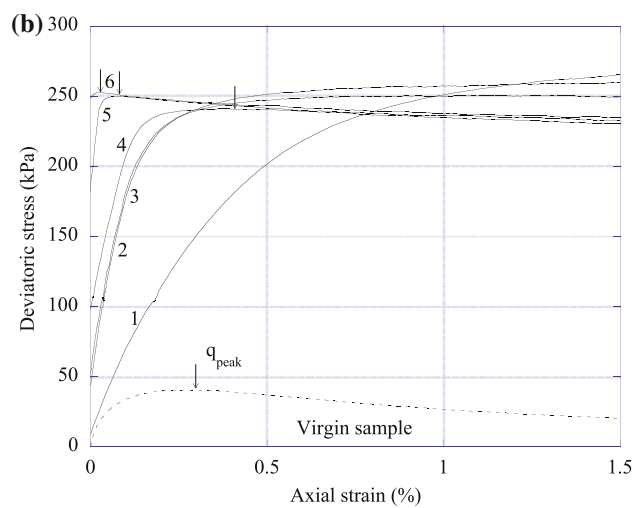
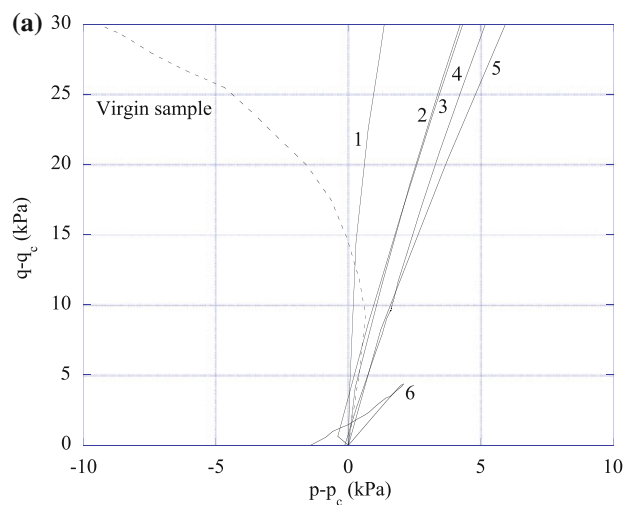


Fig. 9 Detailed results on compression presheared cycle $\eta_{mob} = 1.40$ samples. **a** Effective stress paths. **b** Stress–strain relationships. **c** Pore pressure generation

The effective stress paths are shown in Fig. 8a and separately in two groups for clarity. The first group of 3 tests including $\eta_c = \eta_{mob}$, without drained unloading in Fig. 10, indicates a lightly temporarily unstable behaviour with sharp deviatoric stress peaks, and the second group of also 3 tests including $\eta_c = 0$, with complete drained unloading in Fig. 11, a complete stable behaviour with continuous dilatancy without peaks. In both groups, the effective stress paths no longer develop in parallel pattern in their early stage, contrasting sharply with three precedent series. The close-up view in Fig. 9a shows a vertical initial gradient of test C 1.40–C1 with an inclination towards the positive p' axis indicating a maximum effect of induced anisotropy created by the previous compression preshear cycle, with a greater stiffness in the vertical direction, Graham and Houlsby [16].

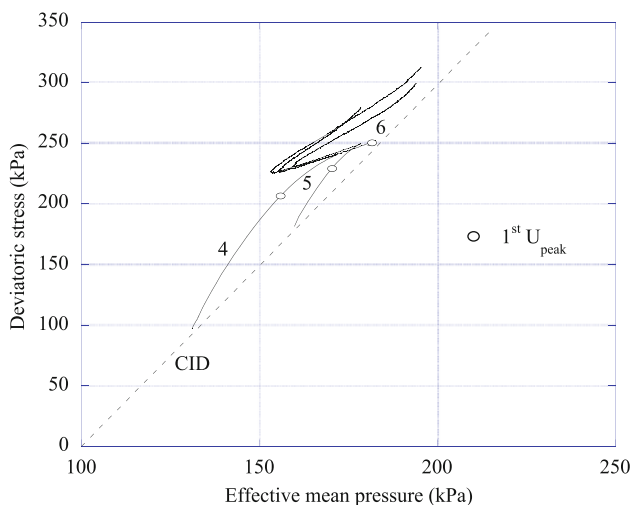


Fig. 10 Effective stress paths with sharp peak for $\eta_{mob} = 1.40$ and high levels of η_c

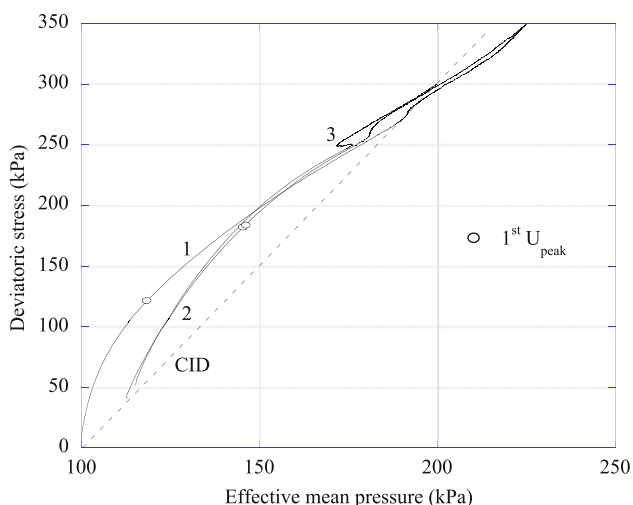


Fig. 11 Effective stress paths without peak for $\eta_{mob} = 1.40$ and small levels of η_c

A very sharp deviatoric peak is noticed for the first time for test C 1.40–C6 without drained unloading. The small open circles in these figures locate the appearance of the first local peak of ΔU at small strain in the effective stress paths. Its location moves rapidly towards the deviatoric peak, as η_c decreases to zero. It means a surprising tendency to dilate within the pseudo-elastic and non-linear domain.

The progressive transition from the temporarily unstable behaviour towards a stable one, in the sense of Hill [19], with the positiveness of d^2W usually associated with dense sand is demonstrated in Fig. 8b, and the remarkable disappearance of the peak in the stress–strain relationship in Fig. 9b. A plateau of deviatoric stress is even detected with test C 1.40–C3 with $\eta_c = 0.44$. The effects of previous stress history are still effective at large strain, since no common portion of stress–strain curve is identified. Test C 1.40–C1 with a complete drained unloading to the initial isotropic stress state has the smallest undrained modulus and the highest development at large strain.

Figure 8c indicates a complex evolution of ΔU with a 2nd local peak (vertical arrows) in the range of 4 to 5% of axial strain and an identical pore pressure gradient at large strain. The values of 2nd local peak decrease strongly with the size of η_c . As η_c approaches zero, the 2nd local peak becomes flatter and the pore pressure development enters the negative domain. These peaks identify the phase transformation. The sharpness and continuous decreasing value of the 1st local peaks at small strain, in the range of only 0.1%, is shown in Fig. 9c.

4 Undrained behaviour analysis

In the rest of this paper, we develop some missing traits linking the observed behaviours of $\eta_c = \eta_{mob}$, without drained unloading to those of $\eta_c = 0$, with complete drained unloading. We try to examine some experimental striking features within the light of elastoplasticity framework : **(O1)** the initial gradient of the effective stress paths, **(O2)** the surprising common response and its curvature, **(O3)** the progressive appearance of dilatancy, **(O4)** the evolution of the undrained behaviour.

4.1 Initial gradient of effective stress paths

Current mainstream of elasto-plasticity theory can offer a plausible explanation for the unexpected initial inclination of the effective stress path in the case of complete drained cycle preshear, $\eta_c = 0$. In Fig. 12, the initial yield surface f for virgin loose sand sample is pushed outward from the first drained triaxial loading to point C of mobilized stress ratio level η_{mob} . The theoretical yield surface f can be approximated as the shape of the effective stress path [34].

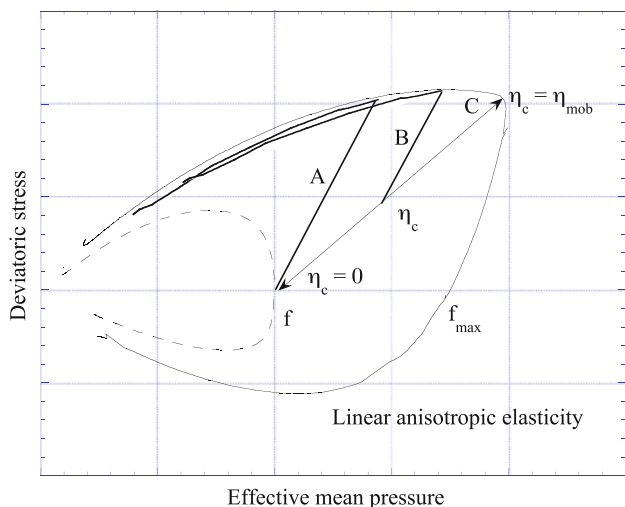


Fig. 12 Qualitative elastoplastic analysis

Subsequent drained unloading from η_{mob} to η_c makes the state of stress enter the yield surface, leaving the actual yield surface f_{max} associated with η_{mob} unchanged. Since the plastic axial strains of the drained unloading are negligible, the sample can be considered at its elastic state at the beginning of the undrained shearing at η_c and the effective stress path can be conveniently modelled using the linear anisotropy elasticity theory. The inclination of the initial gradient of the effective stress path towards the positive p' axis indicates an induced anisotropy created by the previous compression preshear, with a greater stiffness in the vertical direction, Graham and Houlsby [16]. Consequently, parallel and inclined effective stress paths are obtained inside the pseudo-elastic domain from η_c to f_{max}, and the effective stress paths for loose sand follow f_{max} afterwards. This qualitative analysis concerns the case of small η_{mob} not far from the instability line η_{LI}. Non-linear anisotropic elasticity with non-constant parameters can simulate the strong curvature of the observed effective stress paths in the case of high η_{mob}.

Figure 13 shows the initial gradient of the effective stress path for all tests in this study. Excepting the test C 1.40–C1 with a complete drained unloading, a simple linear correlation between the initial gradient and η_c is found, independently of the deviatoric stress q_{mob} or the mobilized stress ratio level η_{mob} attained during the drained compression. Previous study with η_c = 0 [17] suggests that induced anisotropy is initiated solely by the direction of the previous linear stress history. This paper logically adds a linear decreasing of the initial gradient with η_c, due to the presence of a deviatoric stress q_c.

4.2 Pseudo-elastic response

As stated in Fig. 12, the actual yield surface f_{max} associated with past deviatoric stress q_{mob} was left unchanged during

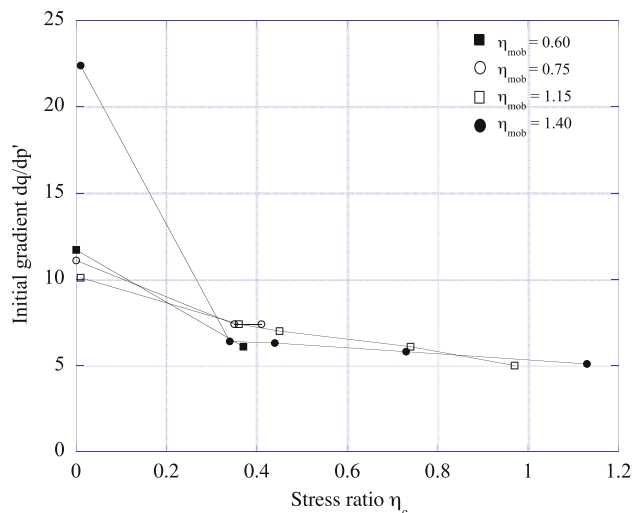


Fig. 13 Initial gradient of effective stress paths

the drained unloading towards η_c. For the first three tested series, all effective stress paths are linear and parallel from η_c to q_{peak} for small mobilized stress ratio level η_{mob}, and non-linear and also parallel for larger mobilized level. Therefore, the first section of AB in Fig. 2 of the effective stress path is termed the pseudo-elastic response inside the past maximum yield surface f_{max}.

The size of this pseudo-elastic domain can be very large, nearly up to q_{peak}, compared to the much more smaller size of the prevailing elastic domain, Tatsuoka et al. [37], Stallebrass and Taylor [35]. The measured axial strain associated with this pseudo-elastic domain has a large value, of about 0.077% for test C 0.75–C1, following the graphical determination shown in Fig. 21. The pseudo-elastic strain is normally obtained with local strain measurements such as non-contact displacement transducers or small LVDT sensors. Unfortunately, the usual local strain sensors are simply too heavy for loose sand samples in this study.

Figure 14 shows the size of the pseudo-elastic domain for all studied series, measured as axial strain and graphically determined using the procedure developed in Sect. 4.5. The linear decreasing of the pseudo-elastic size in series with small η_{mob} and its highly non-linear variation with large η_{mob} suggest the term “pseudo-elastic”. Note for the largest series with η_{mob} = 1.40, the pseudo-elastic axial strain practically coincides with the local minimum of the excess pore pressure, shown in Fig. 18, between the first local maximum indicating the maximum size of the pseudo-elastic domain at small to medium strain and the last local maximum at large strain of the Phase Transformation (PT) line.

A simple experimental correlation between the size of the pseudo-elastic domain and stress ratio η_c is found :

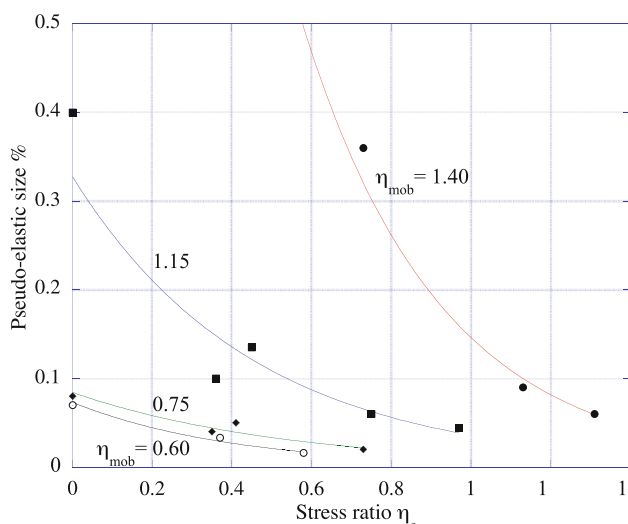


Fig. 14 The size of pseudo-elastic domain

$$\text{Size} = \alpha * \exp(\beta * \eta_c) \tag{1}$$

Best-fitted curve (full line in Fig. 14) with all experimental data points of each series is constructed with excellent coefficient of correlation (more than 0.96). The first coefficient α gives the maximum size of the pseudo-elastic domain occurring when $\eta_c = 0$ and the second coefficient β the reduction in this size with the mobilized level η_{mob} .

For the largest compressive presheared series C 1.40 in Figs. 10 and 11, it is worth emphasizing the strong curvature of the common pseudo-elastic part AB of the effective stress paths towards the positive p' axis. The first maximum local of generated pore pressure within the pseudo-elastic response at medium strains, less than 0.2%, vertical arrows in Fig. 9c and open circles in Fig. 10, occurs well before the second usual maximum local at large strains which reveals the appearance of the PT line.

4.3 Progressive appearance of dilatancy

The second section BC of Fig. 2 begins from q_{peak} at point B to the PT line at point C. The rounded peak of the effective stress paths for small and medium η_{mob} transforms into a very sharp bend for higher η_{mob} of Fig. 10 and even disappears for highest mobilized level η_{mob} and lowest η_c of Fig. 11. Therefore, in term of elastoplasticity analysis, the transition from elastic to plastic behaviour can be smooth or abrupt. The descending part BC after the sharp bend moves upwards with increasing q_{mob} , together with a strong decrease in its length. Regardless of the unloading level η_c , q_{peak} appears to be initiated at a stress state closer to the PT line, as η_{mob} increases. The stress paths move upwards in the section CD towards the

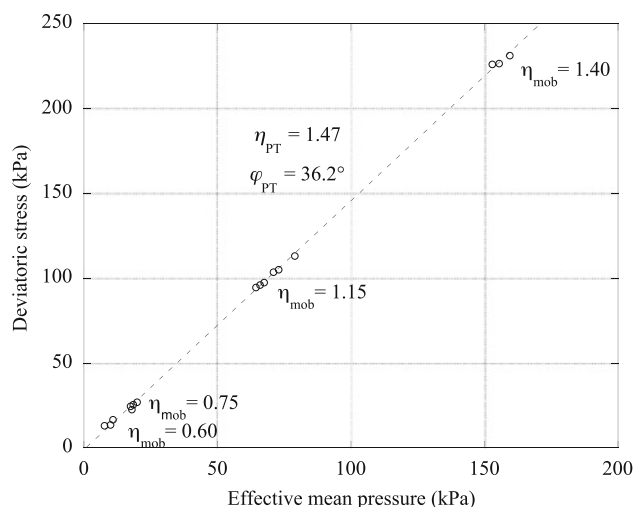


Fig. 15 Phase transformation line of presheared and loose sand

undrained failure line. The final point D can be higher than q_{peak} for large η_{mob} , offering a very similar stable behaviour of dense sand, in the sense of Hill, while being in a loose state. However, the stress path never reaches again the PT line, even at large strain.

The existence of a common and unique PT line for all presheared series is shown in Fig. 15 with $\eta_{PT} = 1.47$ or a mobilized friction angle at PT state $\phi_{PT} = 36.2^\circ$. The concept of Phase Transformation line [29, 36] developed initially for dense sand seems to apply for loose presheared sand. This particular feature indicates the possibility of having an intrinsic nature of the Phase Transformation, independent of past history, as that of failure.

Figure 16 illustrates the typical evolution of the normalized pore pressure versus the mobilized level η_{mob} . This unusual representation can separate the crowded effective stress curves during the final static liquefaction stage near the origin of the $q - p'$ plane. From the mobilized level η_c on the horizontal axis, all undrained tests follow an initial linear (resp. non-linear) part for small (resp. large) η_{mob} evolving in a regular and parallel pattern inside the pseudo-elastic domain. Then, undrained tests follow another set of non-linear, regular, and parallel pattern up to ΔU_{max} . This graph reveals the progressive appearance of the dilatancy phenomenon, since the position of ΔU_{max} moves progressively from $\eta = 1.37$ of the first and second series towards the PT line.

For clarity, the data for fixed undrained level $\eta_c = 0$ are shown separately in Fig. 17. All tests with different fixed mobilized levels η_{mob} , up to 1.40 have a complete drained compression preshear cycle and follow a common non-linear part starting from the origin of the axes; the subsequent evolution is linear and parallel in a regular pattern up to ΔU_{max} . Therefore, the initial common non-linear part is termed pseudo-elastic. It corresponds to the

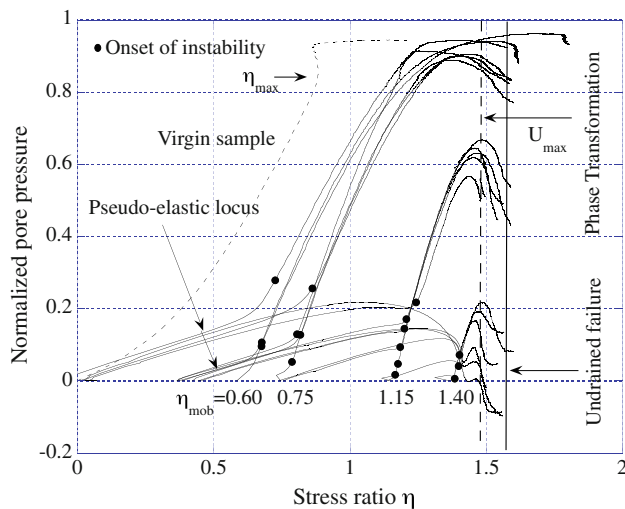


Fig. 16 Progressive appearance of dilatancy

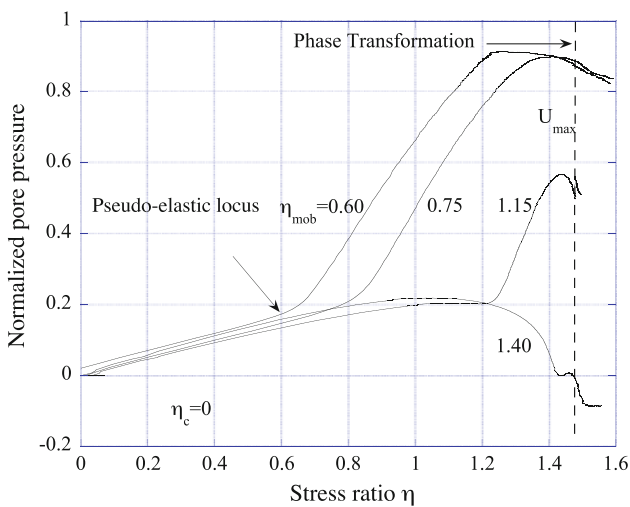


Fig. 17 Response for complete drained compression cycle $\eta_c = 0$

initial non-linear effective stress paths in the $q - p'$ plane. The whole pseudo-elastic domain is revealed with the largest presheared level ($\eta_{mob} = 1.40$) and smallest unloading level ($\eta_c = 0$). The pseudo-elastic domain is highly non-linear with a local peak at about $\eta = 1.15$ in Fig. 16. It means the possibility of decreasing excess pore pressure inside the pseudo-elastic domain, contrasting sharply with the usual increasing of ΔU obtained from the elastic part of the elasto-plastic theory.

Similarly, Fig. 18 shows the data for fixed mobilized level $\eta_{mob} = 1.40$, indicating different pseudo-elastic loci for different undrained levels η_c . As expected for a pseudo-elastic behaviour, they are nearly geometrically similar and the larger the size of the unloading, the bigger the pseudo-elastic domain. The transition from the pseudo-elastic domain to the plastic domain can be smooth as in Fig. 17 or abrupt as in Fig. 18.

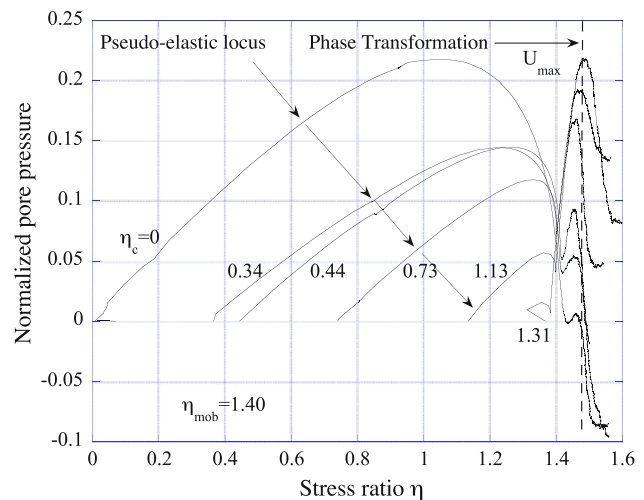


Fig. 18 Response for fixed mobilized level $\eta_{mob} = 1.40$

Once identified the pseudo-elastic locus, the onset of instability for each test is marked with full black circles in Fig. 16. Interestingly, these points are always above the pseudo-elastic locus and move towards the pseudo-elastic locus as η_{mob} increases. It is also worth noting the continuous increase in the stress ratio η , regardless of η_{mob} and η_c , meaning a true hardening behaviour despite a large drop of deviatoric stress in the stress–strain relationship, usually misinterpreted as “strain softening” behaviour of loose sand. This figure indicates a brief softening behaviour for virgin loose sample, since a maximum of stress ratio is observed experimentally at η_{max} (horizontal arrow).

If the instability domain is defined as the region between the PT line and the instability line at peak, then Fig. 19 shows its evolution when examining the effective stress ratio at peak η_{peak} against the mobilization level η_{mob} . This figure shows a gradual reduction in the instability domain with increasing η_{mob} and an asymptotic stabilization towards the line defined by $\eta_{peak} = \eta_{mob}$; however, η_{peak} is always larger than η_{mob} . The stress ratio increment $\Delta\eta = \eta_{peak} - \eta_{mob}$ has a stabilized asymptotic value of about 0.08 before the disappearance of q_{peak} of test C 1.40–C3, in which the common pseudo-elastic curve approaches closely the Phase Transformation Line in Fig. 8a, resulting in a stable behaviour above $\eta_{mob} = 1.35$.

These observations confirm the dependency of the instability concept on the previous preloading history, therefore its well-known non-intrinsic nature [6, 9]. The instability concept also lacks a physical significance, as noted in [2].

4.4 Evolution of undrained strength

The undrained strength of presheared and loose sand in compression, represented by the stress ratio increment

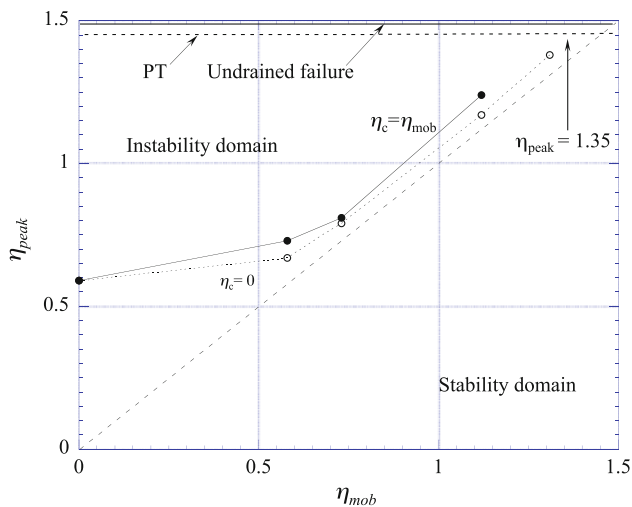


Fig. 19 Instability domain of compression presheared and loose sand

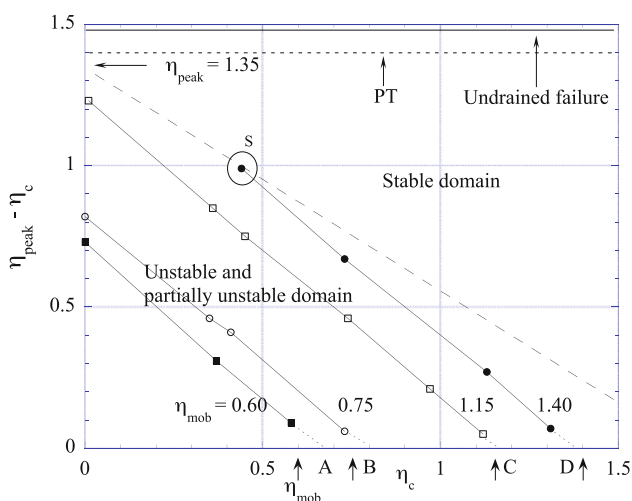


Fig. 20 Stability domain of compression presheared and loose sand

$\Delta\eta = \eta_{peak} - \eta_c$ is plotted in Fig. 20 as function of η_c . The positions of η_{mob} are also indicated on the horizontal axis with four vertical up arrows. Linear decreasing of $\Delta\eta$ with the same gradient was found for each fixed mobilized level η_{mob} , supporting again the existence of pseudo-elastic domain. The intersections of the extrapolated lines with the horizontal axis are noted as points A to D for the four tested series in this paper. Points A and B have larger η value than η_{mob} , meaning the existence of deviatoric peak, regardless of η_c ; therefore, the two series $\eta_{mob} = 0.60$ and $\eta_{mob} = 0.75$ are well inside the unstable domain. Point C is nearly identical to $\eta_{mob} = 1.15$; consequently, the sample C 1.15–C6 with $\eta_c = \eta_{mob}$ is unable to sustain the presence of the deviatoric stress q_c at the beginning of the undrained shearing. Point D is below $\eta_{mob} = 1.40$, signalling the encounter, point S, of the extrapolated lines and the stable

domain. The separation between the unstable and stable domains can be a line passing through point S and point 1.35 on the $\Delta\eta$ axis.

4.5 Synthetic results for undrained behaviour

Figure 21 groups four planes together and shows graphically the relations between all important points of the undrained behaviour of loose sand and drained presheared in compression to η_{mob} and unloaded to η_c . From the beginning of undrained shearing, the first point of interest can be the elastic point (down triangle) having a linear stress–strain relationship. This paper overlooks this elastic domain since no local deformation is used. Leaving the pseudo-elastic domain can be the second encountered point of interest (circle). The pseudo-elastic domain is identified in the lower left graph with a very large η_{mob} and very small η_c . The axial strain associated with the pseudo-elastic domain is surprisingly large, up to 0.077% for the representative test C 0.75–C1; the pseudo-elastic domain surprisingly big, nearly up to deviatoric stress peak, which is the third point (rectangle). This peak initiates the unstable behaviour, in the sense of Hill with negative second-work order, while remaining continuously hardened with increasing mobilized frictional angle. The effects of previous history (stress or strain) are eliminated beyond the fourth point (star). Its range can be large, up to 0.5%. The appearance of dilatancy through the transformation phase is the last point of interest, not shown in the right graphs.

One can identify graphically the position of a particular point of interest, such as the size of the pseudo-elastic domain in term of axial strain, by following a set of three dashed bold lines relating these 4 planes.

4.6 Stress or strain history?

As an example, Fig. 22 shows the effects of recent history on loose sand, starting from an anisotropy stress state at $\eta_c = 0.75$ with three mobilized levels η_{mob} . The main observations (O1) to (O4) obtained initially from an isotropy stress state of previous works can be reasonably extended to any anisotropy stress state.

Since only linear stress paths with fixed direction, $\alpha = 71^\circ$, are considered in this paper, the effects of recent stress history can be examined with only one parameter via the length of the stress path or the stress ratio η_c for any fixed mobilized level η_{mob} .

The undrained shear strength, when it exists, is the most recognized parameter of loose soil behaviour. When examining the deviatoric stress peak expressed as η_{peak} against the recent stress history characterized by η_c , Fig. 23 shows the same slight decrease in η_{peak} for 4 series with

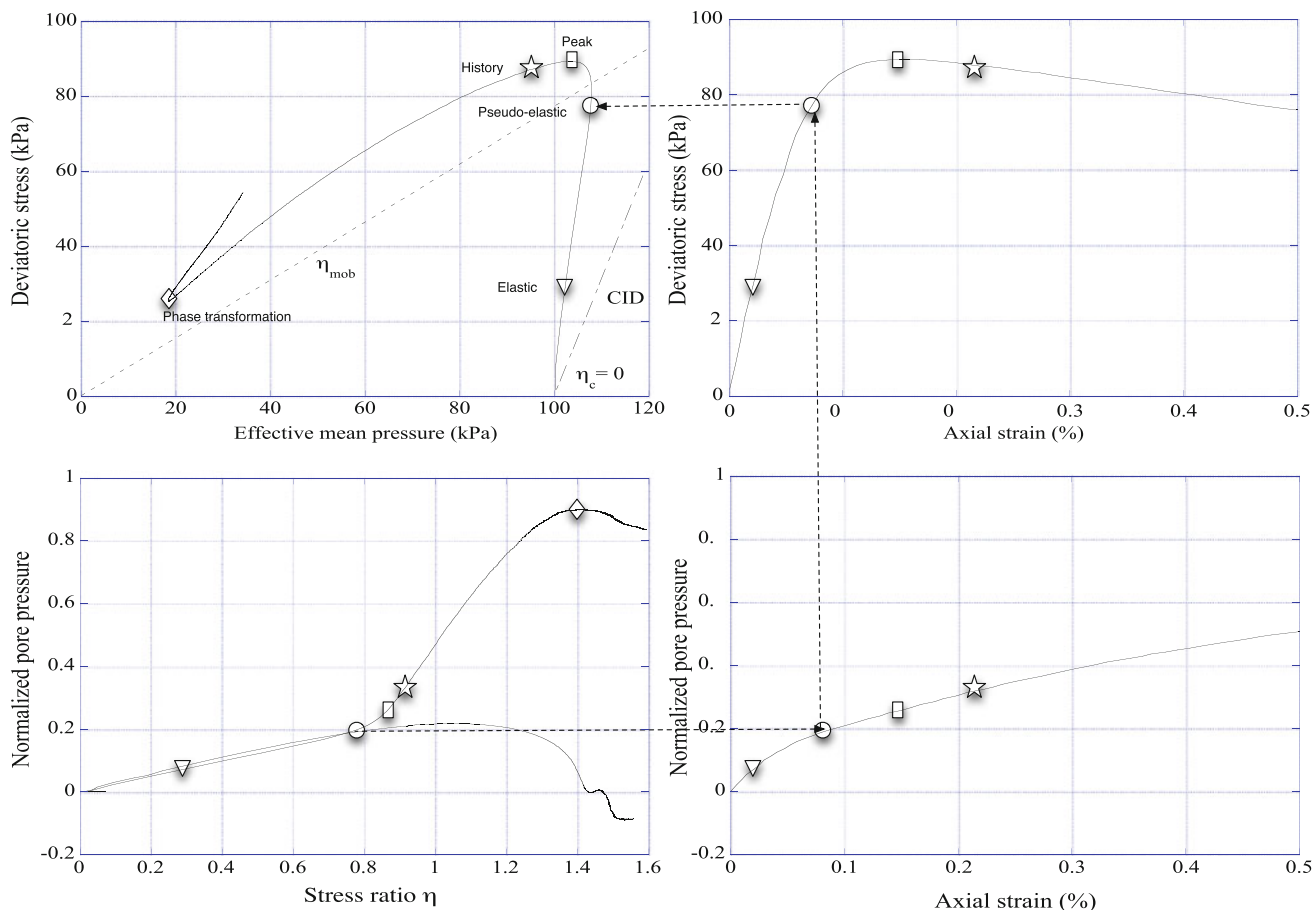


Fig. 21 Graphical identification of points of interest of loose and presheared sand, example of test C 0.75–C1

fixed η_{mob} . In other words, recent stress history affects slightly the soil behaviour, offering very similar effective stress paths and stress–strain relationships in Figs 4 to 9.

Similarly, the effects of recent strain history created by the same linear stress paths can be related to only one parameter, the deviatoric strain ϵ_{dev} , since all samples in this study have nearly the same void ratio prior to undrained loading for a fixed stress ratio level η_c . In Fig. 22 with fixed $\eta_c = 0.75$, very different responses are obtained, ranging from the usual unstable static liquefaction of $\eta_{mob} = 0.75$ to the stable behaviour of dense-like material of $\eta_{mob} = 1.40$. Similar figures with fixed $\eta_c = 0.0$ or 0.35 can be constructed and Fig. 24 indicates a strong and unique evolution of undrained shear strength, or a representative of the effects of deviatoric strain history. The undrained shear strength is regulated essentially by ϵ_{dev} in a simple logarithmic correlation, independently of η_c ; therefore, it seems that deviatoric strain history is the most important component of the undrained induced anisotropy created by linear stress paths in the classical triaxial plane. The stress induced anisotropy Ψ_σ can be neglected with respect to the strain induced anisotropy Ψ_ϵ .

5 Conclusions

This paper presents a detailed study of the undrained triaxial compression behaviour of very loose and saturated Hostun RF clean sand samples prepared by moist tamping technique. It examines the possibilities offered by previous history created by simple linear stress paths with partially drained unloading from a mobilized stress ratio η_{mob} to η_c to explore the effects of undrained induced anisotropy. It contributes to the traits explaining the progressive transformation of compressive and unstable behaviour of loose sand into a dilative and stable behaviour of dense-like sand by recent history, while being loose. Experimental results from this line of research evidence the important role of the recent deviatoric strain history, from any initial isotropic or anisotropic stress state.

Based on a limited number of experiments, the following conclusions extending the history mechanisms of previous studies can be formulated:

1. The initial effective stress gradient at the beginning of the undrained shearing appears to depend only on the

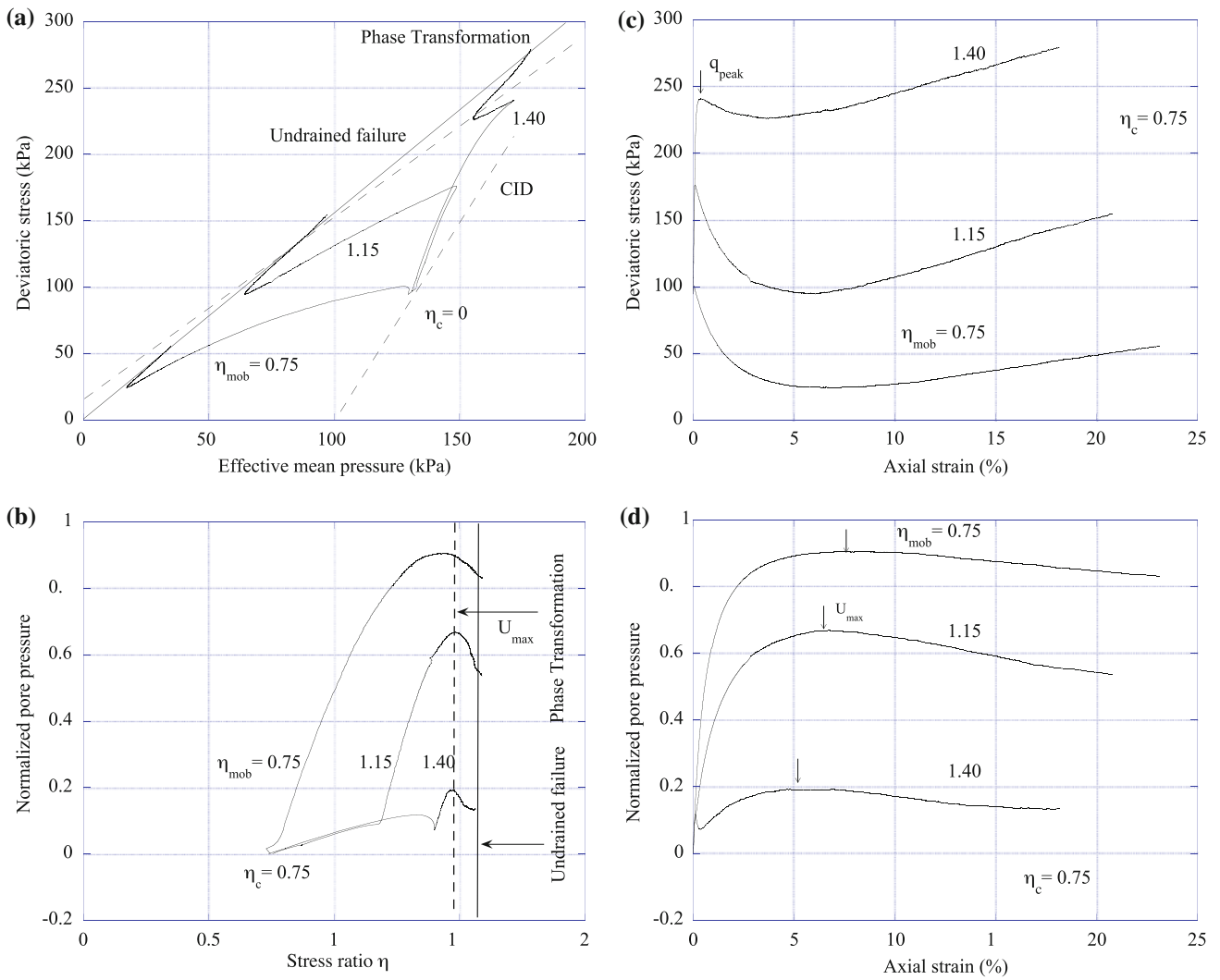


Fig. 22 Results on compression presheared cycle $\eta_c = 0.75$ samples. **a** Effective stress paths. **b** Mobilized level. **c** Stress-strain relationships. **d** Pore pressure generation

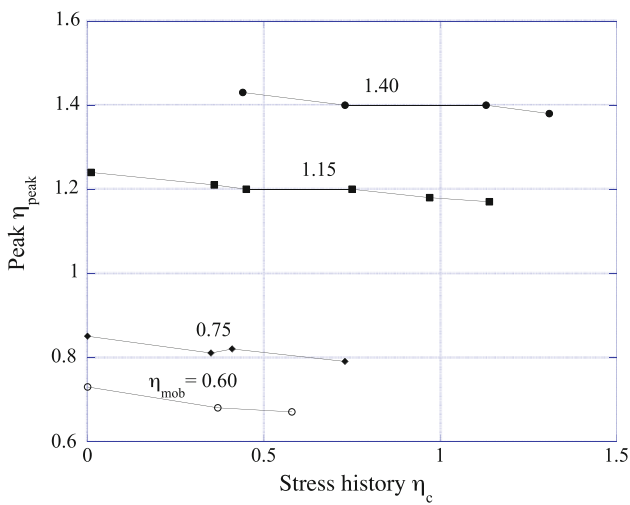


Fig. 23 Stress history

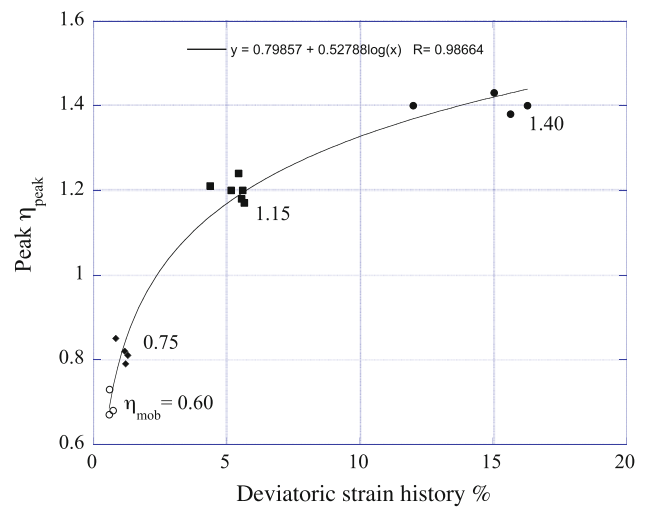


Fig. 24 Strain history

initial stress ratio η_c , irrespective of the mobilized stress ratio level η_{mob} . Furthermore, it depends only on the direction of the previous linear stress path, irrespective of its length. The pseudo-elastic domain, up to the deviatoric stress peak, depends on the mobilized stress ratio level η_{mob} and on stress ratio η_c before the final undrained shearing in compression. A graphical procedure for identification of points of interest is formulated.

2. All effective stress paths are linear and parallel from η_c to q_{peak} for small mobilized stress ratio level η_{mob} , and non-linear and also parallel for larger mobilized level.
3. The quantitative determination of the effects of previous stress history as function of mobilized stress ratio level η_{mob} : for small η_{mob} , previous history can be erased beyond 0.3 to 0.5% of axial strain; and for large η_{mob} , previous history can not be eliminated.
4. The progressive appearance of dilatancy phenomenon is function of mobilization level η_{mob} , resulting in a common and unique Phase Transformation line for all presheared series of loose sand. It seems that the concept of Phase Transformation can be regarded as intrinsic.
5. The hardening property of the static liquefaction phenomenon, despite the large drop of the deviatoric stress in the stress–strain relationship, is often misinterpreted as “strain softening” behaviour of loose sand in the geotechnical literature.

The last experimental observation leaves an open question : can loose sand experience a true softening behaviour associated with the drop of deviatoric stress in the stress–strain relationship, together with a decreasing mobilized frictional angle? Additional experiments on various sands are currently investigated to address this issue.

The experimental data can be downloaded from the journal website, or on request to the first author.

Acknowledgments Part of this work was done with the financial support of the MENRT (French Educational Ministry of Research and Technology) to the third author. Special thanks are also due to Mrs. M.C. Jean for reviewing the draft version.

References

1. Arthur JRF, Menzies B (1972) Inherent anisotropy in a sand. *Géotechnique* 22(2):115–128
2. Been K, Jefferies MG (2004) Stress-dilatancy in very loose sand. *Can Geotechnical J* 41(5):972–989
3. Bjerrum L, Kringstad S, Kummeneje O (1961) The shear strength of a fine sand. In: *Proceedings of the 5th International Conference Soil Mechanical Foundation Engineering*, vol. 1, pp. 29–37
4. Canou J, Thorel L, De Laure E (1991) Influence d'un déviateur de contrainte initial sur les caractéristiques de liquéfaction statique du sable. In: *Proceedings of X ECSMFE, Firenze*, vol. 1, pp. 49–52
5. Darve F, Servant G, Laouafa F, Khoa HDV (2004) Failure in geomaterials : continuous and discrete analyses. *Comput Methods Appl Mech Eng* 193(27):3057–3085
6. Di Prisco C, Matiotti R, Nova R (1995) Theoretical investigation of the undrained stability of shallow submerged slopes. *Géotechnique* 45(3):479–496
7. Doanh T, Finge Z, Boucq S Effects of previous deviatoric strain histories on the undrained behaviour of Hostun RF loose sand. Submitted 0(0):0–0
8. Doanh T, Ibraim E (2000) Minimum undrained strength of Hostun RF. *Géotechnique* 50(4):377–392
9. Doanh T, Ibraim E, Matiotti R (1997) Undrained instability of very loose Hostun sand in triaxial compression and extension. Part 1: experimental observations. *Mech Cohes Friction Mater* 2(1):47–70
10. Finge Z (2004) Contribution à l'étude du comportement non drainé des sables lâches surconsolidés et anisotropes. Thèse de doctorat, Institut National des Sciences Appliquées de Lyon
11. Finge Z, Doanh T, Dubujet Ph (2006) Undrained anisotropy of Hostun RF loose sand : new experimental hints. *Can Geotech J* 43(11):1195–1212
12. Flavigny E, Desrues J, Palayer B (1990) Le sable Hostun RF. *Revue Française de Géotechnique* 53: 67–69
13. Frost JD, Park JY (2003) A critical assessment of the moist-tamping technique. *Geotech Test J* 26(1):57–70
14. Gajo A, Piffer L (1999) The effects of preloading history on the undrained behaviour of saturated loose sand. *Soil Found* 39(6):43–54
15. Georgiannou VN, Burland JB, Hight DW (1990) The undrained behaviour of clayey sands in triaxial compression and extension. *Géotechnique* 40(3):431–449
16. Graham J, Houlsby GT (1983) Anisotropic elasticity of a natural clay. *Géotechnique* 33(2):165–180
17. Hareb H (2009) Contribution à l'étude des effets des histoires de préchargement sur le comportement à la liquéfaction des sables très lâches. Thèse de doctorat, Institut National des Sciences Appliquées de Lyon
18. Hight DW, Gens A, Symes MJ (1983) The development of a new hollow cylinder for investigating the effects of principal stress rotation in soils. *Géotechnique* 33(4):355–384
19. Hill R (1958) A general theory of uniqueness and stability in elastic plastic solids. *J Mech Phys Solids* 6: 236–249
20. Ibraim E (1998) Différents aspects du comportement des sables à partir des essais triaxiaux: des petites déformations à la liquéfaction statique. Thèse de doctorat, Institut National des Sciences Appliquées de Lyon
21. Ishihara K (1996) *Soil behaviour in earthquake geotechnics*. Oxford University Press, Oxford
22. Ishihara K, Okada S (1978) Effects of stress history on cyclic behaviour of sand. *Soil Found* 18(4):31–45
23. Ishihara K, Okada S (1978) Yielding of overconsolidated sand and liquefaction model under cyclic stresses. *Soil Found* 18(1):57–72
24. Ishihara K, Okada S (1982) Effects of large preshearing on cyclic behaviour of sand. *Soil Found* 22(3):109–125
25. Konrad JM (1993) Undrained response of loosely compacted sands during monotonic and cyclic compression tests. *Géotechnique* 43(1):69–89
26. Ladd RS (1978) Preparing test specimens using undercompaction. *Geotech Test J* 1(1):16–23
27. Lade PV, Nelson RB, Ito YM (1988) Instability of granular materials with nonassociated flow. *J Eng Mech ASCE* 114(12):2173–2191

28. Lanier J, Di Prisco C, Nova R (1993) Etude expérimentale et analyse théorique de l'anisotropie induite du sable Hostun. *Revue Française de Géotechnique* (57):59–74
29. Luong MP (1978) Etat caractéristique du sol. *C.R.A.S. B*, 287: 305–307
30. Matiotti R (1996) Analisi sperimentale del fenomeno della liquefazione statica delle sabbie sciolte e sue applicazioni numeriche. Phd Thesis, Politecnico di Milano
31. Meghachou M (1992) Stabilité des sables lâches : essais et modélisation. Thèse de doctorat, Université scientifique et médicale de Grenoble
32. Poorooshasb HB, Holubec I, Sherbourne AN (1966) Yielding and flow of sand in triaxial compression: part 1. *Can Geotech J* 3(4):179–190
33. Poorooshasb HB, Holubec I, Sherbourne AN (1967) Yielding and flow of sand in triaxial compression: part 2 and 3. *Can Geotech J* 4(4):376–397
34. Reza Imam SM, Morgenstern NR, Robertson PK, Chan DH (2002) Yielding and flow liquefaction of loose sand. *Soil Found* 42(3):19–31
35. Stallebrass SE, Taylor RN (1997) The development and evaluation of a constitutive model for the prediction of ground movements in overconsolidated clay. *Géotechnique* 47(2):235–254
36. Tatsuoka F, Ishihara K (1974) Yielding of sand in triaxial compression. *Soil Found* 14(2):63–76
37. Tatsuoka F, Sato T, Park CS, Kim YS, Mukabi JN, Kohata Y (1994) Measurements of elastic properties of geomaterials in laboratory compression tests. *Geotech Test J* 17(1):80–94
38. Touron G (2007) Effets de l'histoire de préchargement sur le comportement à la liquefaction du sable d'Hostun RF. Master de recherche, ENSMSE - ENISE
39. Vaid YP, Chung EKF, Kuerbis RH (1989) Preshearing and undrained response of sands. *Soil Found* 29(4):49–61
40. Wood DM (1994) General report: Evaluation of material properties. In: Miura S, Shibuya S, Mitachi T (eds) *Proceedings of Pre-failure deformation of geomaterials*, Sapporo, Japan, vol. 2. Balkema, Rotterdam, pp 1179–1199